One Ligand, Four Cages: Diverse Outcomes in Pd_3L_4 Metal-Peptidic Cage Self-Assembly *via* Subtle Oligoproline Modifications

Ben E. Barber,[1,2,3] Ellen M. G. Jamieson, [1,2,3] Leah E. M. White, [1,2,3] and Charlie T. McTernan[1,2,*]

[1]Artificial Molecular Machinery Laboratory, The Francis Crick Institute, 1 Midland Road, London NW1 1AT, UK. [2]Department of Chemistry, King's College London, Britannia House, 7 Trinity Street, London SE1 1DB, UK. [3]Authorship is alphabetical. [*]Corresponding Author

KEYWORDS: supramolecular chemistry, metal-organic cage, metal-peptidic cage, self-assembly, proline, PPII, tetra-pyridyl palladium, isomer control, regioselectivity, anisotropy, peanut, peptide, catenane, mechanically interlocked

ABSTRACT: The self-assembly of metal-organic cages enables the rapid creation of atomically defined, three-dimensional, nanoscale architectures from easily accessible building blocks. Rigid and flat aromatic panels are typically used as ligands. Building on our recent success using oligoprolines to create defined metal-peptidic Pd_2L_4 cages with emergent head-to-tail isomer control, we have defined a new family of metal-peptidic cages. Herein, we show that installation of an additional metal-binding motif, enabling formation of Pd_3L_4, dual-cavity, anisotropic 'peanut' cages, generates complex and emergent behavior in response to small changes in ligand isomerism. By varying the sequence isomer used, or the stereochemistry of the 4*R*/*S* hydroxyproline, we can generate four distinct self-assembly outcomes, forming: the Pd_3L_4 *cis CCNN* cage isomer, the Pd_3L_4 'All Up' *CCCC* cage isomer, a mixture of all possible isomers of Pd_3L_4 cages, or an interpenetrated Pd_6L_8 cage. We show that simple and subtle changes to a peptidic ligand give rise to complex behavior in metal-peptidic cage self-assembly, further underlining the advantages of supramolecular chemistry embracing biological building blocks.

INTRODUCTION

Metal-organic cages are discrete, three-dimensional species formed from the self-assembly of metal ions with rigid, organic ligands.[1-3] A variety of polyhedra with defined internal cavities can be readily formed, and the function of these systems stems from the dramatically different properties of the internal cavity from the surrounding solution.[4,5] Metal-organic cages have been shown to perform challenging separations,[6] catalyze reactions at rates comparable to enzymes,[7-9] act as contrast agents or transport cargoes *in vivo,*[10-12] and sequester contaminants.[13,14] Flat, aromatic, panels are often used to provide the structural rigidity required to favor the self-assembly of defined, discrete species.[15] This leads to two key problems; firstly, water solubility can be challenging and stability limited, due to the fundamental propensity of building blocks to drop out of solution.[16] Secondly, functionalization of the internal cavity, where the most interesting properties of the cages lie, is challenging and few examples have been reported.[17-19]

Creating anisotropic cavities has been an area of increasing interest, as researchers seek to move away from the pseudo-spherical cavities of current generation of metal-organic capsule, towards systems better able to mimic the selectivity and potency of biological systems.[20] The use of less symmetric ligands, and heteroleptic systems, have provided routes to lower symmetry cages with augmented properties.[21] However, they are still bounded by the limitations of aromatic and conjugated building blocks. Creating functional, and particularly chiral, cage cavities remains challenging.[22,23]

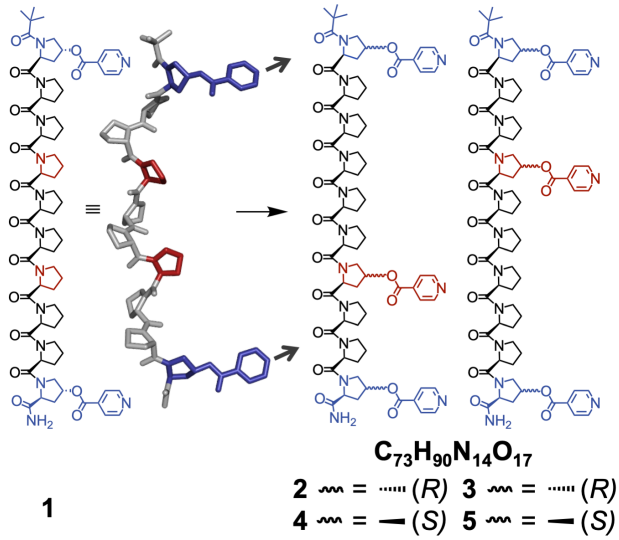

Figure 1. a. Oligoproline ligand used to assemble a Pd_2L_4 metal-peptidic cage in our previous work. Residues on the n and n+3 are aligned on the same face of the helix, allowing installation of metal binding groups at the 1st and 10th residue.[27,28] **b**. Additional modification at the 4th or 7th residues with 4*R*/*S* hydroxyproline creates tritopic ligands for Pd_3L_4 cage self-assembly.

One way to functionalize the interior of metal-organic cages is to use tritopic, linear, ligands to create differentiated cavities in a single assembly in 'peanut' cages.[24, 25] However, the assembly of 'peanut' cages from low symmetry ligands is rare, limiting their anisotropy. Lewis and co-workers have reported a

pseudo-heteroleptic Pd_3L_4 cage formed from a single asymmetric ligand, with geometric complementarity and restrictions leading to self-assembly of a single cage isomer.[26] The anisotropy of such cages is limited, however, by the planarity and lack of chirality of the planar building blocks.

To address these challenges with solubility, biocompatibility, and anisotropy, we recently reported a new class of metal-organic cages – metal-peptidic cages – formed from oligoproline ligands, whose defined folding in solution provides the requisite rigidity for the formation of discrete species.[27] Oligoproline peptides reliably form a left-handed polyproline II (PPII) helix in aqueous solutions, which contains all *trans*-amide bonds.[28,29] This secondary structure has a rigid helical structure with a repeat length of 9 Å, with every third residue aligned on the same face of the helix, and tolerates substitution.[30-33] This creates a platform for intrinsically water-soluble cages whose interior can easily be functionalised.[34] We demonstrated that a family of Pd_2L_4 cages of different sizes could be readily formed, and that the rich, chiral, helical, surfaces of these cages led to unusual host-guest behavior. We also found that the use of complex, chiral, helical, building blocks led to the unexpected emergence of isomer control, with the *cis CCNN* head-to-tail isomer of cage formed exclusively (**Figure 2A**).[35] More recently, a preprint has reported a modified system using alternative linkers to pyridines – highlighting the robustness of the oligoproline platform.[36]

Herein, we use the helical nature, and modular synthesis, of oligoprolines to design cages with multiple internal cavities, and to control head-to-tail isomerism, by installing additional metal coordinating residues. Using intrinsically tuneable subcomponents, and automated synthesis, provides a unique platform for the synthesis of tritopic building blocks for Pd_3L_4 cages.[37] Fine adjustments to the structure can be made by changing peptide sequence and/or point chirality of amino acid building blocks. This allows us to precisely adjust the relative location and geometry of metal-binding motifs along the peptidic backbone. We hypothesized that such adjustments would enable us to control the outcome, and head-to-tail isomerism, of metal-peptidic cage assembly. We find that we can create differentiated, highly anisotropic, cavities, and that highly complex behavior can be generated from simple changes to peptide sequence isomers and/or point stereochemistry (**Figure 2B**). Four isomers of a single ligand deliver four unique outcomes – a *cis CCNN* Pd_3L_4 cage, an 'All Up' *CCCC* Pd_3L_4 cage, a mixture of all possible Pd_3L_4 cage isomers, and an interpenetrated Pd_6L_8 cage – demonstrating the flexibility and power of using complex chiral building blocks in supramolecular chemistry.

RESULTS AND DISCUSSION

We have previously used helical PPII oligoproline strands with ten residues, formed by solid phase peptide synthesis, to build metal-peptidic Pd_2L_4 cages.[27] We initially decided to target the installation of an additional metal binding site within the cavity in an attempt to override the intrinsic preference of our Pd_2L_4 systems to form *cis CCNN* cages. We reasoned that an asymmetrically aligned additional binding site (**Figure 1**) would favor the 'All Up' *CCCC* isomer, as the only way to achieve coordinative saturation.

To form Pd_3L_4 cages, we used the alignment of every third residue on the same face of the helix in an ideal PPII structure.[28] As we aimed to synthesize Pd_3L_4 cages with anisotropic cavities, we based our design on the 10mer peptide coupled to isonicotinic acid ^{t}BuCO$_2$-(Hyp)-(Pro)$_8$-(Hyp)-CONH$_2$ (**1**) we have previously used to synthesize Pd_2L_4 cage **6**$(BF_4)_4$. In the 10mer peptide **1**, positions 1, 4, 7 and 10 are aligned, and can be functionalized with metal binding residues. Pro-4 is nearer to the *N*-terminus, and Pro-7 is nearer to the *C*-terminus. Each could be changed to Hyp as a precursor for a tritopic ligand and, due to the directionality of the PPII helix, led to two ligand structural isomers (**Figure 1**). We expected these systems to act identically, as installation of the additional binding site was anticipated to force the 'All Up' *CCCC* isomer, with the smaller of the two cavities either towards the *N*-terminus or the *C*-terminus.

We synthesized ^{t}BuCO$_2$-(Hyp)-(Pro)$_5$-(Hyp)-(Pro)$_2$-(Hyp)-CONH$_2$ and its structural isomer ^{t}BuCO$_2$-(Hyp)-(Pro)$_2$-(Hyp)-(Pro)$_5$-(Hyp)-CONH$_2$ using solid phase peptide synthesis (SPPS), and coupled them with isonicotinic acid to yield **2** and **3** respectively. The peptides were subsequently purified by preparatory high-performance liquid chromatography (Prep-HPLC). In **2**, the internally substituted proline/binding motif is closer to the *C*-terminus (Pro-7) whereas in **3** it is closer to the *N*-terminus (Pro-4). The *tert*-butyl carbonyl group provides additional PPII stability,[38] and a distinct NMR handle for cage assembly and isomer formation assignment (**Figure 2B**). Folding to a PPII conformation in **2** and **3** in H_2O was confirmed by CD spectroscopy, showing characteristic minima and maxima at *c.* 205 and 225 nm (**Figure 3E**).[39]

With the ligands in hand, we assembled cages by adding $Pd(CH_3CN)_4(BF_4)_2$ in a precisely 4:3 ligand:metal ratio to each of **2** and **3**. We found that strict stoichiometric control was essential to reproducibly assemble cages.[27] Discrete species **7** and **8** were formed in each case (**Figure 3A** + **3B**), with downfield shifts in the pyridyl protons indicative of palladium(II) co-ordination, and desymmetrization of ligand signals along the oligoproline backbone. Interestingly, while **2** assembled into a sharply resolved single species **7**, analogous to our previously reported Pd_2L_4 systems,[27] assemblies of **3** to form **8** showed much more complex behavior. The ^{1}H NMR of both assemblies also showed changes over time, with initially broad signals sharpening over five days at room temperature (Figure S99 – S102). This indicates that the self-assembly process faces a higher energetic barrier to equilibration than our Pd_2L_4 cages, which were equilibrated within five minutes. We attribute this to the costs of breaking additional coordination bonds (*vide infra*).

We collected ^{1}H NMR, ^{13}C, correlated spectroscopy (COSY), heteronuclear single quantum coherence spectroscopy (HSQC), heteronuclear multiple bond correlation spectroscopy (HMBC), DOSY, ESI-HRMS, Ion Mobility Mass Spectrometry (IMMS) and CD data on the successful assemblies, all of which were consistent with the formation of metal-peptidic cages. The 1D and 2D NMR spectra of **7** show formation of a single, well resolved, species, with a two-fold desymmetrisation of ligand signals. Spectra of **8** are complex (Figures S52 – S58), but clearly show that multiple different spin systems and isomers are formed. DOSY spectra showed a single diffusion band for **7** and **8**, with a hydrodynamic radius approximately twice that of the free ligand (**Figure 3C**), consistent with cage assembly.[40] Hydrodynamic radii of 24.0 Å (**7**) and 28.3 Å (**8**) were in-line with our previously reported hydrodynamic radii and computational modelling (*vide infra* and SI Section 10). High resolution electrospray mass spectroscopy (ESI-HRMS) showed clean formation of cage, with dominant $Pd_3L_4^{6+}$ and $Pd_3L_4(BF_4)^{5+}$ peaks for **7** and **8**, and isotopic distributions matching simulations, consistent with successful Pd_3L_4 formation (**Figure 3D**).

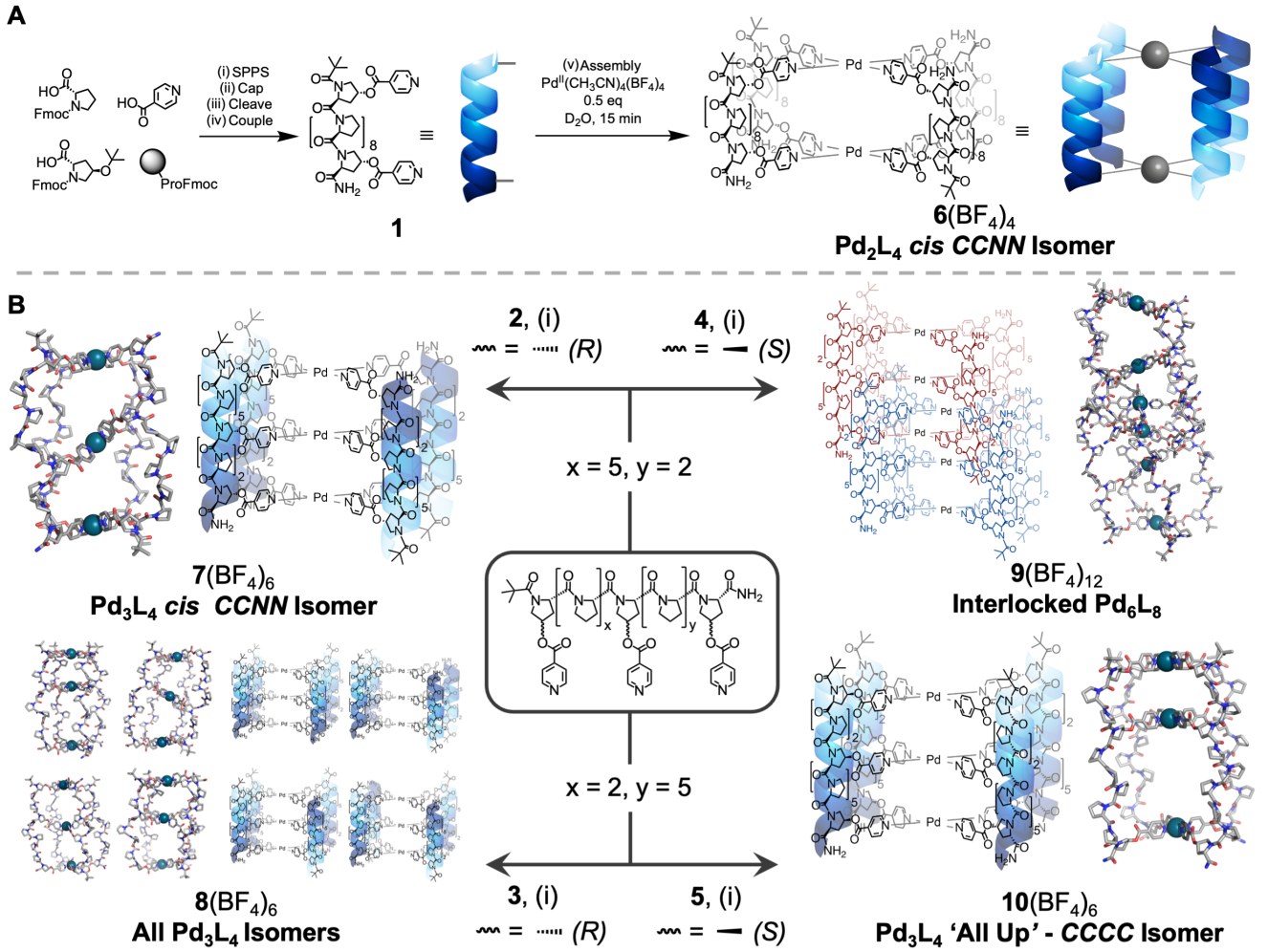

Figure 2. a. Synthesis of 10mer oligoproline ligand **1** and its self-assembly into Pd_2L_4 metal-peptide cage **6** in our previous work.[27] (i) Solid-phase peptide synthesis (see supplemental information for protocol). (ii) Pivalic anhydride:CH_2Cl_2:DMF 1:4.5:4.5, r.t., 45 min. (iii) Trifluoroacetic acid:triisopropyl silane:H_2O 38:1:1, r.t, 2 h. (iv) EDCI (6 equiv), DMAP (3 equiv), isonicotinic acid (6 equiv), CH_2Cl_2, r.t., 16 h (v) $Pd(CH_3CN)_4(BF_4)_2$ (0.5 eq), D_2O, r.t., 15 mins. **b**. Oligoproline ligands **2** - **5** designed in this paper, and the self-assembly outcomes demonstrated in this work. (i) $Pd(CH_3CN)_4(BF_4)_2$ (0.75 eq), D_2O, r.t., 5 days.

IMMS showed peaks at a collision cross-section of 1046 Å^2 and 1076 Å^2 for **7** and **8**, consistent with previous results for Pd_2L_4 species **6** (Figure S103 and S104).[27,41] CD confirmed retention of the PPII structure of ligands **2** and **3** on cage assembly (**Figures 3E**, S107 +108).

Our ligands are intrinsically directional (the *C*-terminus is distinct from the *N*-terminus), and so there are four different head-to-tail cage isomers that can form, even though our cages are homoleptic (**Figure 2B**).[35,42,43] The *C*-termini can all be aligned at one end and bind one palladium(II) ion of the cage (the 'All Up' *CCCC*), three *C*-termini and one *N*-terminus can lie at one end (the *CCCN*), and there are two cases where two *C*-termini and two *N*-termini are at each end, either with *C* termini *cis* or *trans* to each other across the palladium(II) center (*cis CCNN* and *trans CNCN*, respectively). We have previously reported that ester-functionalized ditopic oligoproline ligands with *N*-terminal *tert*-butyl carbonyl capping groups give a strong preference for *cis* cage assembly.[27]

To assign which cage isomer was formed in each Pd_3L_4 self-assembly, we considered the number of ligand environments that would arise in the ^{1}H NMR due to desymmetrisation imposed by bringing chiral, helical, oligoprolines into close proximity (SI Section 9). Both the 'All Up' *CCCC* and *trans CNCN* isomers contain just one ligand environment, while the *cis CCNN* isomer contains two, and the 'Three Up' *CCCN* isomer contains four separate environments (Figure S121). This provides eight distinct ligand environments, if all isomers are simultaneously present. The *tert*-butyl protons H_ε provide a valuable handle, as they are well resolved and isolated from overlapping signals, providing a clear indication of the isomer(s) of cage formed, with each signal corresponding to a different ligand environment. **7** showed two distinct ligand environments in ^{1}H NMR (**Figure 3A**), with two singlets for the *tert*-butyl protons H_ε, and 12 doublets for aromatic protons H_α and H_β (with some partial overlap), consistent with formation of the *cis CCNN* isomer. This assignment is further supported by NOESY analysis (Figure S122 & 123), which enabled us to confirm that each pyridine H_α sees two, but not three, other pyridine environments (see SI Section 9 for a detailed discussion of our reasoning). As such, we assign **7** as a *cis CCNN* Pd_3L_4 cage.

The ^{1}H NMR spectrum for **8** is more complex (**Figure 3B**), but clearly resolves eight major *tert*-butyl signals, indicative of eight different ligand environments (Figure S124). This is further supported by analysis of the aromatic pyridine H_α and H_β protons (Figure S121), showing a similar increase in

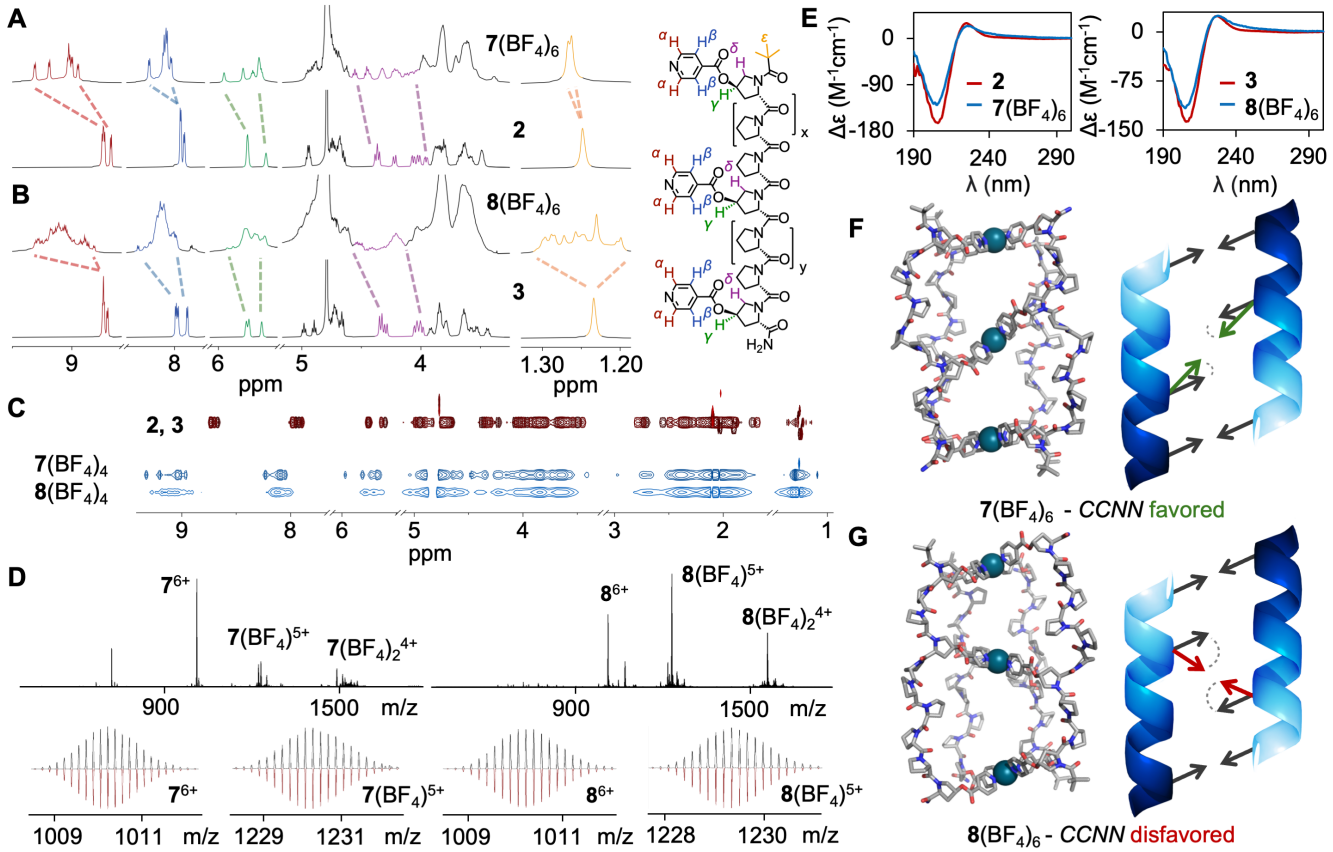

Figure 3. a. ^{1}H NMR (600 MHz, D_2O, 298 K) of cage **7**$(BF_4)_6$ (top) and ligand **2** (bottom) **b**. ^{1}H NMR (600 MHz, D_2O, 298 K) of cage **8**$(BF_4)_6$ (top) and ligand **3** (bottom) **c**. ^{1}H DOSY NMR (600 MHz, D_2O, 298 K) of ligands **2**, **3** (red) and cages **7**$(BF_4)_6$ and **8**$(BF_4)_6$ (blue) **d**. ESI-HRMS data of cages **7**$(BF_4)_6$ (left) and **8**$(BF_4)_6$ (right) and their isotopic distributions (recorded top, simulated bottom) **e**. Circular dichroism of ligands **2**, **3** (red) and cages **7**$(BF_4)_6$ and **8**$(BF_4)_6$ (blue) **f.** Side view of **7**$(BF_4)_6$ *cis CCNN* isomer molecular model (left) and stylized representation with distortions of central co-ordination vector highlighted in green (right) **g.** Side view of **8**$(BF_4)_6$ *cis CCNN* isomer molecular model (left) and stylized representation with distortions of central co-ordination vector highlighted in green (right).

identifiable environments. As we did not observe other major species by ESI-HRMS (Figure S60) and observe a single species by DOSY, we assigned these ligand environments to multiple cage isomers being present in solution. To observe eight different environments, all four cage isomers must be present, thus demonstrating a total lack of isomer selectivity. Attempts to synthesize cage **8** at a lower temperature did not result in a significantly different spectra/ratio of species. (Figure S88).

We had initially predicted that installing additional metal coordinating residues in ligands **2** and **3**, as compared to the base ditopic 10mer **1**, would favor formation of the 'All Up' *CCCC* arrangement. This arrangement would position the internal pyridines of each oligoproline in the same plane, preorganising them to coordinate a third Pd(II), generating Pd_3L_4 cages with two asymmetric cavities (Figure S133). However, this is not consistent our observations for **7** and **8**. Our Pd_2L_4 cages displayed an inherent energetic preference for the *cis CCNN* isomer, and our additional modifications are fighting this intrinsic bias (See SI Section 10 for further discussion). **7** was able to form the preferred *cis CCNN* isomer; however, with **8**, a mix of all four isomers was formed. We attribute this to a greater deformation of the central binding site required on assembly, and so a greater energetic penalty for formation of the *cis CCNN* isomer using **3**, which raises the energy of the *cis* such that there is no significant energy difference between isomers (**Figure 3F** vs **G**).

We sought to obtain crystallographic data to better understand the difference in cage isomer selectivity between **2** and **3**. However, despite extensive attempts (>200 per sample), we did not obtain crystals suitable for X-ray diffraction, consistent with previously reported difficulties in crystallizing PPII structures.[27] Therefore, we undertook molecular modelling studies to gain additional insight into the underlying causes.

Our previous studies of Pd_2L_4 systems indicated that the *cis CCNN* cage isomer adopted a tilt, where the helical axis of the oligoproline rods was not perpendicular to the pyridine co-ordination vector (**Figure 1**), which significantly decreased the energy of the *cis CCNN* relative to the other isomers. Therefore, when considering the favorability of the *cis CCNN* isomer for cages **7** and **8**, we need to consider the effect of this tilt on the alignment of the additional, internal, metal coordination sites. As the internal metal coordination site is located asymmetrically along the oligoproline backbone, its coordination vector can no longer be parallel to those at the *N*- and *C*-termini in the *cis CCNN* isomer. This prevents the central $PdPyr_4$ plane from lying parallel to the terminal planes in the Pd_3L_4 structure. In **2**, the distortion required is smaller, and in the same direction as already required for the terminal coordination vectors (**Figure 3F** vs **G**, and SI Section 10). In contrast, the distortion in **3** is larger and in the opposite direction to that of the terminal coordination vectors, which would require significant backbone or metal binding site distortion (**Figure 3F** vs **G**). Modelling of **7** shows that the lowest energy isomer of the cage is the tilted *cis CCNN*, with a distortion of the internal palladium co-ordination plane resulting in

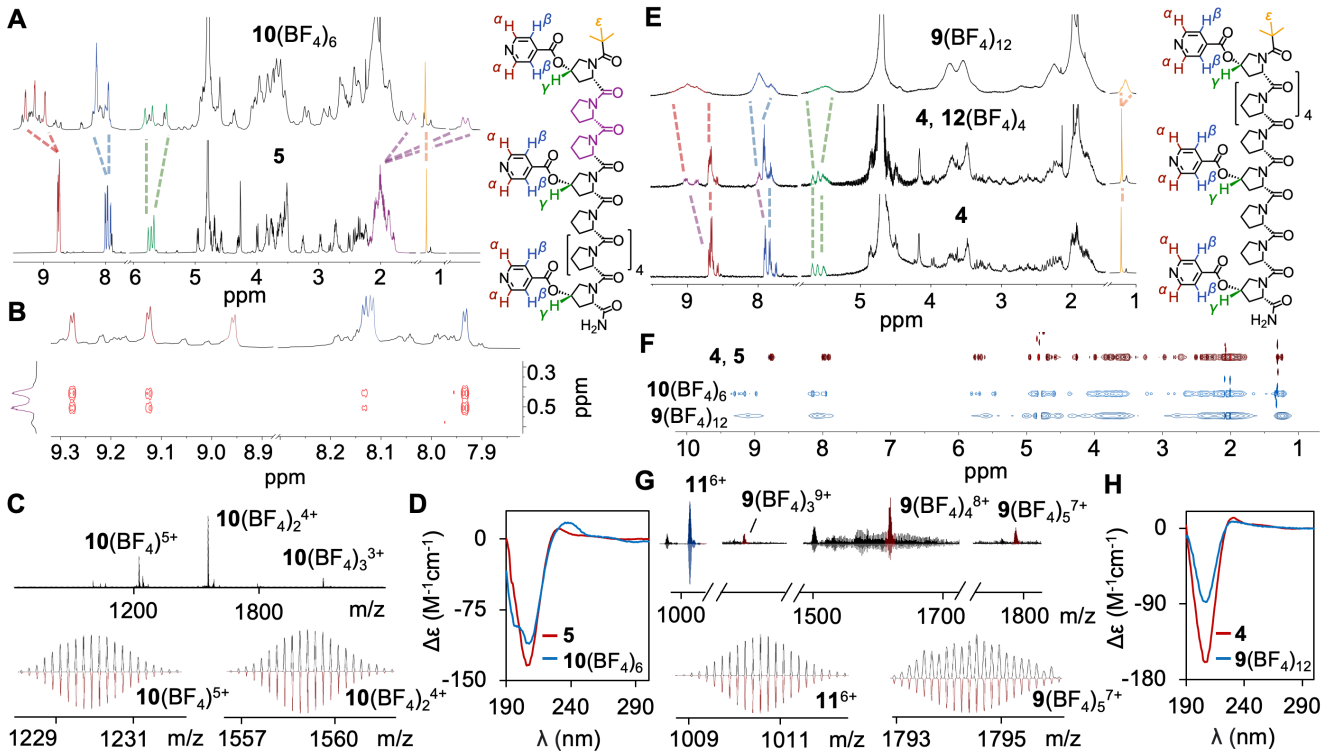

Figure 4. a. ^{1}H NMR (600 MHz, D_2O, 298 K) of cage **10**$(BF_4)_6$ (top) and ligand **5** (bottom) **b.** ^{1}H NOESY NMR (950 MHz, D_2O, 298 K) showing correlations between downfield shifted proline backbone peaks and two of three H_α and H_β environments. **d.** ESI-HRMS data of **10**$(BF_4)_6$ with isotopic distributions (recorded top, simulated bottom) **e.** Circular dichroism of ligand **5** (red) and cage **10**$(BF_4)_6$ (blue) **f.** ^{1}H NMR (600 MHz, D_2O, 298 K) of interlocked cage **9**$(BF_4)_{12}$ (top), ligand **4** with 0.6 eq $Pd(CH_3CN)_4(BF_4)_2$ with intermediate **12**$(BF_4)_4$, a Pd_2L_4 species highlighted in purple (middle) and ligand **4** (bottom) **f.** ^{1}H DOSY NMR (600 MHz, D_2O, 298 K) of ligands **4**, **5** (red) and cages **9**$(BF_4)_6$ and **10**$(BF_4)_{12}$ (blue) **g.** ESI-HRMS data of **9**$(BF_4)_6$, showing loss of interlocked species peaks relative to Pd_3L_4 cage **11**, with isotopic distributions (recorded top, simulated bottom) **h.** Circular dichroism of ligand **4** (red) and cage **9**$(BF_4)_{12}$ (blue).

the formation of two symmetric cavities (**Figure 3F**, S131 and 132). Computational models of the *cis CCNN* isomer of **8** were less able to adopt the stabilizing tilt, and gave a higher energy structure, with similar energy levels to the *trans CNCN*, 'All Up' *CCCC* and 'Three Up' *CCCN* isomers (SI Section 10). This supports our observation of the formation of all possible isomers by ^{1}H NMR.

The contrast of the self-assembly of **2** to give a single Pd_3L_4 cage isomer, and its structural isomer **3** to form all possible head-to-tail isomers, was striking. Therefore, we sought to control and expand this selectivity further. Having explored the effect of positional isomerism, we decided to investigate the effect of the point chirality at the 4-position of the Hyp residues, moving from *R* to *S*. As **2** and **3** showed that the tilt of the co-ordination vectors relative to the polyproline helical axis dictated isomer control, we reasoned that inverting the stereocenter directly attached to the metal binding unit could have a drastic effect. We hypothesized that this would force the coordinating vectors in the opposite direction relative to the oligoproline helical vector. We initially hypothesized that such a switch, from 4*R* to 4*S* stereocenters, would invert the preference for isomer control for each structural isomer: the diastereomer of **2** would form a mix of all 4 possible isomers rather than selective *cis CCNN* isomer, and the diastereomer of **3** would form the *cis CCNN* isomer rather than a mix of all 4 possible isomers.

Ligands **4** and **5** (**Figure 1**), which are diastereoisomers of **2** and **3** respectively, with 4*S*-hydroxyprolines in place of 4*R*, were readily synthesized on resin, demonstrating the modularity and tunability of our approach (**Figure 2B**). We observed additional peaks in the ^{1}H NMR spectra of both ligands (Figures S125 + 126). As the purity of **4** and **5** was >98% by liquid chromatography mass spectrometry (LCMS) (Figures S28 + S38), we attribute these peaks to a subpopulation of ligand containing *cis* amide bonds, estimated by NMR to be <10% of the total. This was confirmed by CD spectroscopy, in which we observed a reduction in the characteristic PPII peaks for both **4** and **5** relative to **2** and **3** (**Figure 4D + H**, S111, S113, S115). 4*S*-Hyp electron withdrawing substituents are known to destabilize PPII helices,[44,45] inducing an endo-ring pucker that destabilizes *trans* amide bonds. In contrast, 4*R*-Hyp preferentially adopts an exo ring pucker which stabilizes *trans* amide bonds by $n\rightarrow\pi^*$ interactions.[45,46] Therefore, introduction of unnatural 4*S*-Hyp residues in ligands **4** and **5** was expected to have a destabilizing effect on the PPII structure, explaining the small reduction in PPII signals seen in the CD spectra of the ligands. As such, we expected **4** and **5** to behave differently in self-assembly due to inversion of individual stereocenters, and distortions from idealized PPII structures.

Ligand **5**, the diastereomeric complement of **3**, was assembled with $Pd(CH_3CN)_4(BF_4)_2$ in a precisely 4:3 ligand:metal ratio, and characterized by ^{1}H NMR, DOSY NMR, IMMS, and ESI-HRMS (Figure **4**), which were consistent with metallopeptidic cage assembly. The ^{1}H NMR yielded a sharp and discrete major species, in contrast to the mixture of cage isomers observed in the self-assembly of **3** (**Figure 4A**). DOSY showed a single diffusion band, indicating formation of a single species with a hydrodynamic radius of 28.3 Å (**Figure 4B**). ESI-HRMS confirmed successful self-assembly of a

Pd_3L_4 cage **10**, with **10**$(BF_4)^{5+}$ and **10**$(BF_4)_2^{4+}$ peaks dominant, and isotopic distributions matching simulations (**Figure 4F**, S85 – S87). IMMS showed a peak for **10** at a collision cross-section of 1023 Å^2, consistent with previous results (Figure S106).

The major species of **10** consists of a single ligand environment, and not the characteristic doubling of ligand environments on self-assembly we have previously observed for *cis CCNN* metal-peptidic cages. Whilst inverting the 4*R*-Hyp stereocenters of **8** enabled the formation of a single isomer, it was not the expected *cis CCNN* isomer. The absence of desymmetrization on cage assembly indicates formation of either an 'All Up' *CCCC* or *trans CNCN* arrangement as the major isomer (see SI Section 9). We attribute the minor species observed in the ^{1}H NMR to small amounts of the remaining 3 isomers, and subpopulations of cages containing *cis* amide bonds, as no other major species were observed by ESI-HRMS (Figure S85). Geometric considerations, and molecular modelling, suggest the formation of the *trans CNCN* isomer would be unfavorable (see SI Section 10 for computational modelling), without extensive loss of PPII folding, which is not observed by CD (**Figure 4D**), and analysis of the NOESY correlations further supports this assignment.

The NOESY spectrum of **10** shows strong correlations between protons of two of the three pyridines and proline sidechains of the backbone. (**Figure 4B**, S128 + S129), which we have not observed in other systems. This supports the assignment of the major product as an 'All Up' *CCCC* isomer, where the smaller cavity of the cage partially contracts, forcing the pyridines and the oligoproline backbone into close proximity in the cavity (see SI Section 9 for further reasoning and explanation). We also observe significant upfield shifts of the α, β and γ protons of Pro2/Pro3, consistent with close contacts between Pro2/Pro3 and the aromatic ring current of the pyridine (**Figure 4A**). We would not expect to see this pattern of NOESY correlations in the *trans CNCN* isomer, supporting our assignment of the *CCCC* 'All Up' isomer (see SI Section 9 for detailed reasoning). We hypothesize that the most likely mechanism involves concertinaing of one cavity of **10**, between the *N*-terminal Hyp and its neighboring Hyp. This hypothesis is supported by the significant changes shown in the CD of **10** as compared to the free ligand **5** (**Figures 4D**, S110), and the appearance of new absorbances (the characteristic PPII peak at 230 nm shifts and broadens to 238 nm) which do not correlate with PPII, PPI, or unstructured peptide.[36,44] We assign these to the concerted concertinaing of **10**, with correlated interactions between the pyridine and proline residues driving changes in CD absorbance. Given the decrease in PPII helical character (as assayed by ^{1}H NMR and CD, Figures S115 & S125) in ligand **5** as compared to ligand **3**, we believe this process is mediated by *trans* to *cis* isomerism of some amide bonds along the proline backbone, localized in the smaller cavity of the cage, which contains a higher local concentration of PPII-destabilizing 4*S*-Hyp.

Whilst the change in isomer selectivity surprised us, we were pleased to find that flipping the 4*R*-Hyp stereocenters of **3** does indeed lead to self-assembly of a single Pd_3L_4 cage isomer using the diastereomeric ligand **5**. This novel 'All Up' *CCCC* isomer has two separate and highly distinctive cavities, achieving one the initial aims of our research.

We then investigated self-assembly of **4**, the diastereomer of **2**. As **2** self-assembled to give only the *cis CCNN* Pd_3L_4 isomer, we expected its diastereomer **9** to self-assemble to give a mixture of cage isomers, reversing the pattern seen for the 4*R*-Hyp cages **7** and **8**. Self-assembly of **4** with $Pd(CH_3CN)_4(BF_4)_2$ in a precisely 4:3 ligand:metal ratio gave a single, broad species in the ^{1}H NMR spectra (**Figure 4E**). ESI-HRMS showed the unexpected formation of both Pd_3L_4 and Pd_6L_8 species (**Figure 4G**, S71-S76). DOSY NMR showed self-assembly of a single species with a hydrodynamic radii of 33.3 Å (**Figure 4F**), larger than the hydrodynamic radii seen for the three Pd_3L_4 cages **7**, **8** and **10** (24.0 – 28.3 Å), consistent with the formation of a larger metal-peptidic structure, and with our modelling studies (Section S10).

We assigned this to an interpenetrated Pd_6L_8 cage **9** formed by the interlocking of two Pd_3L_4 cage (**11**) complexes. Interpenetrated cage structures have been reported, often driven by exclusion of solvent from cavities.[48-50] We attributed the broadness in the ^{1}H NMR both to the increased molecular weight leading to decreased tumbling, but also to the presence of catenation isomers, as there are numerous ways for two cage species, assembled from four tripodal ligands with helical and point chirality, to interlock. To confirm that **9** was indeed an interpenetrated cage, we undertook dilution studies, as monomeric cages should be favored at higher dilution (**Figure 4G**, S71 + S72). We found that dilution of the Pd_6L_8 cage **9** led to the disappearance of peaks corresponding to the catenane, leaving the Pd_3L_4 cage **11**$^{6+}$ peaks unchanged, supporting our assignment of **9** as an interpenetrated species.[50,51]

To probe the self-assembly of the interpenetrated Pd_6L_8 cage **9**, we carried out titrations of diastereomers **2** and **4** with $Pd(CH_3CN)_4(BF_4)_2$ (SI Section 5). We followed partial assemblies by ^{1}H NMR (Figures S89 + S90) and ESI-HRMS (Figures S93 + S94), and found that **2** self-assembles into the *cis CCNN* Pd_3L_4 cage at sub-stoichiometric quantities, forming the free ligand and fully assembled cage, indicating a level of cooperativity to cage assembly, as we had observed in our previous oligoproline Pd_2L_4 cages.[27] In contrast, upon addition of sub-stoichiometric quantities of $Pd(CH_3CN)_4(BF_4)_2$, **4** formed a discrete and well-defined intermediate species **12** in the ^{1}H NMR, which broadened as we approached the 4:3 ligand:metal ratio required to form **9** (Figures S91 + S92). This species showed two ligand environments, which is consistent with *cis CCNN* Pd_2L_4 cage formation, and the intermediate's **12**$(BF_4)_4$ stoichiometry was confirmed by ESI-HRMS (Figures S96 + 97). We confirmed Pd_2L_4 cage assembly by DOSY NMR (Figure S98). This suggests that catenation is occurring as a result of filling the final metal coordination site within a pre-formed *cis CCNN* Pd_2L_4 cage.[51] We hypothesize that catenation provides an energetic contribution to offset the distortion of the central metal binding site required for coordination of the third Pd(II). We, therefore, see both the partial collapse of **10** and the catenation of **9** as two different responses to the same stressors – reduction of PPII preference as we move to 4*S*-Hyp, and misalignment of ligand coordination vectors. This subtle variation in adaptation showcases the complex behavior enabled by the use of peptides as building blocks in metal-peptidic cages.

Herein, we have shown that a series of four isomeric oligoproline ligands can be used synthesize Pd_3L_4 metal-peptidic 'peanut' cages. We demonstrate how small changes in ligands, varying structural isomers and point chiral centers, can lead to dramatic changes in self-assembly. Each of the four tritopic ligands produces a different cage upon addition of

Pd(II): **2** forms the *cis CCNN* Pd_3L_4 isomer, **5** forms the 'All Up' *CCCC* Pd_3L_4 isomer, **3** forms all possible Pd_3L_4 isomers simultaneously, and **4** forms a interpenetrated Pd_6L_8 cage, generating a diverse range of anisotropic cavities. Future work will explore how the asymmetric cavities generated can be leveraged for differential guest binding, drug delivery, catalysis and sensing.

ASSOCIATED CONTENT

Supporting Information

The Supporting Information is available free of charge on the ACS Publications website.

Supplemental Information (PDF)

AUTHOR INFORMATION

Corresponding Author

* Corresponding author: Charlie McTernan, charlie.mcternan@crick.ac.uk

Author Contributions

Authorship is alphabetical between B.E.B., E.M.G.J., and L.E.M.W.

Conceptualization, B.E.B., E.M.G.J., L.E.M.W., and C.T.M.; formal analysis, B.E.B., E.M.G.J., and L.E.M.W.; investigation, B.E.B., E.M.G.J., and L.E.M.W.; resources, C.T.M.; writing—original draft, B.E.B., E.M.G.J., L.E.M.W.; writing—review & editing; B.E.B., E.M.G.J., L.E.M.W., and C.T.M.; visualization, B.E.B., E.M.G.J., L.E.M.W., and C.T.M; supervision; C.T.M.; project administration, C.T.M.; funding acquisition, C.T.M.

Funding Sources

This work was supported by the Francis Crick Institute, which receives its core funding from Cancer Research UK (CC2213), the UK Medical Research Council (CC2213), and the Wellcome Trust (CC2213) and by the UKRI under Future Leaders Fellowship MR/W00657X/1. This work was supported by the Francis Crick Institute through provision of access to the MRC Biomedical NMR Centre. The Francis Crick Institute receives its core funding from Cancer Research UK (CC1078), the UK Medical Research Council (CC1078), and the Wellcome Trust (CC1078).

ACKNOWLEDGMENT

We thank Dr. Meng Li, Warwick University, for recording IMMS data, and Dr. Peter Simpson, Dr. Alain Oregioni, and Dr. Geoff Kelly for their advice and support with NMR spectroscopy

ABBREVIATIONS

Hyp, (2*S*, 4*R/S*)-4-Hydroxyproline, COSY, correlated spectroscopy; DOSY, diffusion ordered spectroscopy; ESI-HRMS, electrospray ionization high-resolution mass spectrometry; HMBC, heteronuclear multiple bond correlation spectroscopy; HSQC, heteronuclear single quantum coherence spectroscopy; IMMS, ion-mobility mass spectrometry; LCMS, liquid chromatography mass spectrometry; PPI, polyproline I; PPII, polyproline II; Pro, *L*-proline; ^{t}Bu, *tert*-butyl.

REFERENCES

(1) Seidel, S. R.; Stang, P. J. High-Symmetry Coordination Cages *via* Self-Assembly. *Acc. Chem. Res.* **2002**, *35* (11), 972–983. DOI: 10.1021/ar010142d

(2) Han, M.; Engelhard, D. M.; Clever, G. H. Self-Assembled Coordination Cages Based on Banana-Shaped Ligands. *Chem. Soc. Rev.* **2014**, *43* (6), 1848–1860. DOI: 10.1039/C3CS60473J

(3) Fujita, M.; Ogura, K. Supramolecular Self-Assembly of Macrocycles, Catenanes, and Cages through Coordination of Pyridine-Based Ligands to Transition Metals. *Bull. Chem. Soc. Jpn.* **1996**, *69* (6), 1471–1482. DOI: 10.1246/bcsj.69.1471

(4) Rizzuto, F. J.; Von Krbek, L. K. S.; Nitschke, J. R. Strategies for Binding Multiple Guests in Metal–Organic Cages. *Nat. Rev. Chem.* **2019**, *3* (4), 204–222. DOI: 10.1038/s41570-019-0085-3

(5) Yoshizawa, M.; Kusukawa, T.; Kawano, M.; Ohhara, T.; Tanaka, I.; Kurihara, K.; Niimura, N.; Fujita, M. Endohedral Clusterization of Ten Water Molecules into a "Molecular Ice" within the Hydrophobic Pocket of a Self-Assembled Cage. *J. Am. Chem. Soc.* **2005**, *127* (9), 2798–2799. DOI: 10.1021/ja043953w

(6) Zhang, D.; Ronson, T. K.; Zou, Y.; Nitschke, J. R. Metal–Organic Cages for Molecular Separations. *Nat. Rev. Chem.* **2021**, *5* (3), 168–182. DOI: 10.1038/s41570-020-00246-1

(7) Hastings, C. J.; Pluth, M. D.; Bergman, R. G.; Raymond, K. N. Enzymelike Catalysis of the Nazarov Cyclization by Supramolecular Encapsulation. *J. Am. Chem. Soc.* **2010**, *132* (20), 6938–6940. DOI: 10.1021/ja102633e

(8) Cullen, W.; Misuraca, M. C.; Hunter, C. A.; Williams, N. H.; Ward, M. D. Highly Efficient Catalysis of the Kemp Elimination in the Cavity of a Cubic Coordination Cage. *Nat. Chem.* **2016**, *8* (3), 231–236. DOI: 10.1038/nchem.2452

(9) DiNardi, R. G.; Rasheed, S.; Capomolla, S. S.; Chak, M. H.; Middleton, I. A.; Macreadie, L. K.; Violi, J. P.; Donald, W. A.; Lusby, P. J.; Beves, J. E. Photoswitchable Catalysis by a Self-Assembled Molecular Cage. *J. Am. Chem. Soc.* **2024**, *146* (31), 21196–21202. DOI: 10.1021/jacs.4c04846

(10) Cosialls, R.; Simó, C.; Borrós, S.; Gómez-Vallejo, V.; Schmidt, C.; Llop, J.; Cuenca, A. B.; Casini, A. PET Imaging of Self-Assembled ^{18}F-Labelled Pd_2L_4 Metallacages for Anticancer Drug Delivery. *Chem. Eur. J.* **2023**, *29* (3), e202202604. DOI: 10.1002/chem.202202604

(11) Burke, B. P.; Grantham, W.; Burke, M. J.; Nichol, Gary. S.; Roberts, D.; Renard, I.; Hargreaves, R.; Cawthorne, C.; Archibald, S. J.; Lusby, P. J. Visualizing Kinetically Robust Co^{III}_4 L_6 Assemblies *in Vivo* : SPECT Imaging of the Encapsulated [^{99m}Tc]TcO_4^- Anion. *J. Am. Chem. Soc.* **2018**, *140* (49), 16877–16881. DOI: 10.1021/jacs.8b09582

(12) Sokolow, G. E.; Crawley, M. R.; Morphet, D. R.; Asik, D.; Spernyak, J. A.; McGray, A. J. R.; Cook, T. R.; Morrow, J. R. Metal−Organic Polyhedron with Four Fe(III) Centers Producing Enhanced T_1 Magnetic Resonance Imaging Contrast in Tumors. *Inorg. Chem.* **2022**, *61* (5), 2603–2611. DOI: 10.1021/acs.inorgchem.1c03660

(13) Ronson, T. K.; Carpenter, J. P.; Nitschke, J. R. Dynamic Optimization of Guest Binding in a Library of Diastereomeric Heteroleptic Coordination Cages. *Chem* **2022**, *8* (2), 557–568. DOI: 10.1016/j.chempr.2021.12.017

(14) Percástegui, E. G. Metal–Organic Cages against Toxic Chemicals and Pollutants. *Chem. Commun.* **2022**, *58* (33), 5055–5071. DOI: 10.1039/D2CC00604A

(15) Pullen, S.; Clever, G. H. Mixed-Ligand Metal–Organic Frameworks and Heteroleptic Coordination Cages as Multifunctional Scaffolds—A Comparison. *Acc. Chem. Res.* **2018**, *51* (12), 3052–3064. DOI: 10.1021/acs.accounts.8b00415

(16) Percástegui, E. G.; Ronson, T. K.; Nitschke, J. R. Design and Applications of Water-Soluble Coordination Cages. *Chem. Rev.* **2020**, *120* (24), 13480–13544. DOI: 10.1021/acs.chemrev.0c00672

(17) Tominaga, M.; Suzuki, K.; Murase, T.; Fujita, M. 24-Fold Endohedral Functionalization of a Self-Assembled $M_{12}L_{24}$ Coordination Nanoball. *J. Am. Chem. Soc.* **2005**, *127* (34), 11950–11951. DOI: 10.1021/ja054069o

(18) Johnson, A. M.; Hooley, R. J. Steric Effects Control Self-Sorting in Self-Assembled Clusters. *Inorg. Chem.* **2011**, *50* (11), 4671–4673. DOI: 10.1021/ic2001688

(19) Howlader, P.; Das, P.; Zangrando, E.; Mukherjee, P. S. Urea-Functionalized Self-Assembled Molecular Prism for Heterogeneous Catalysis in Water. *J. Am. Chem. Soc.* **2016**, *138* (5), 1668–1676. DOI: 10.1021/jacs.5b12237

(20) McTernan, C. T.; Davies, J. A.; Nitschke, J. R. Beyond Platonic: How to Build Metal–Organic Polyhedra Capable of Binding Low-Symmetry, Information-Rich Molecular Cargoes. *Chem. Rev.* **2022**, *122* (11), 10393–10437. DOI: 10.1021/acs.chemrev.1c00763

(21) Pullen, S.; Tessarolo, J.; Clever, G. H. Increasing Structural and Functional Complexity in Self-Assembled Coordination Cages. *Chem. Sci.* **2021**, *12* (21), 7269–7293. DOI: 10.1039/D1SC01226F

(22) Suzuki, K.; Kawano, M.; Sato, S.; Fujita, M. Endohedral Peptide Lining of a Self-Assembled Molecular Sphere to Generate Chirality-Confined Hollows. *J. Am. Chem. Soc.* **2007**, *129* (35), 10652–10653. DOI: 10.1021/ja073629b

(23) Tang, X.; Jiang, H.; Si, Y.; Rampal, N.; Gong, W.; Cheng, C.; Kang, X.; Fairen-Jimenez, D.; Cui, Y.; Liu, Y. Endohedral Functionalization of Chiral Metal-Organic Cages for Encapsulating Achiral Dyes to Induce Circularly Polarized Luminescence. *Chem* **2021**, *7* (10), 2771–2786. DOI: 10.1016/j.chempr.2021.07.017.

(24) Yazaki, K.; Akita, M.; Prusty, S.; Chand, D. K.; Kikuchi, T.; Sato, H.; Yoshizawa, M. Polyaromatic Molecular Peanuts. *Nat. Commun.* **2017**, *8* (1), 15914. DOI: 10.1038/ncomms15914.

(25) Preston, D.; Lewis, J. E. M.; Crowley, J. D. Multicavity $[Pd_nL_4]^{2n+}$ Cages with Controlled Segregated Binding of Different Guests. *J. Am. Chem. Soc.* **2017**, *139* (6), 2379–2386. DOI: 10.1021/jacs.6b11982

(26) Lewis, J. E. M. Pseudo-heterolepticity in Low-Symmetry Metal-Organic Cages. *Angew. Chem. Int. Ed.* **2022**, *61* (44), e202212392. DOI: 10.1002/anie.202212392

(27) Barber, B. E.; Jamieson, E. M. G.; White, L. E. M.; McTernan, C. T. Metal-Peptidic Cages—Helical Oligoprolines Generate Highly Anisotropic Nanospaces with Emergent Isomer Control. *Chem* **2024**, *10* (9), 2792–2806. DOI: 10.1016/j.chempr.2024.05.002

(28) Wilhelm, P.; Lewandowski, B.; Trapp, N.; Wennemers, H. A Crystal Structure of an Oligoproline PPII-Helix, at Last. *J. Am. Chem. Soc.* **2014**, *136* (45), 15829–15832. DOI: 10.1021/ja507405j

(29) El-Baba, T. J.; Fuller, D. R.; Hales, D. A.; Russell, D. H.; Clemmer, D. E. Solvent Mediation of Peptide Conformations: Polyproline Structures in Water, Methanol, Ethanol, and 1-Propanol as Determined by Ion Mobility Spectrometry-Mass Spectrometry. *J. Am. Soc. Mass Spectrom.* **2019**, *30* (1), 77–84. DOI: 10.1007/s13361-018-2034-7

(30) Kümin, M.; Sonntag, L.-S.; Wennemers, H. Azidoproline Containing Helices: Stabilization of the Polyproline II Structure by a Functionalizable Group. *J. Am. Chem. Soc.* **2007**, *129* (3), 466–467. DOI: 10.1021/ja067148o

(31) Dobitz, S.; Aronoff, M. R.; Wennemers, H. Oligoprolines as Molecular Entities for Controlling Distance in Biological and Material Sciences. *Acc. Chem. Res.* **2017**, *50* (10), 2420–2428. DOI: 10.1021/acs.accounts.7b00340

(32) Lewandowska, U.; Zajaczkowski, W.; Chen, L.; Bouillière, F.; Wang, D.; Koynov, K.; Pisula, W.; Müllen, K.; Wennemers, H. Hierarchical Supramolecular Assembly of Sterically Demanding π-Systems by Conjugation with Oligoprolines. *Angew. Chem. Int. Ed.* **2014**, *53* (46), 12537–12541. DOI: 10.1002/anie.201408279.

(33) Brightwell, D. F.; Truccolo, G.; Samanta, K.; Shepherd, H. J.; Palma, A. Supramolecular Self-Assembly of Engineered Polyproline Helices. *ACS Macro. Lett.* **2023**, *12* (7), 908–914. DOI: 10.1021/acsmacrolett.3c00304

(34) Pandey, A. K.; Naduthambi, D.; Thomas, K. M.; Zondlo, N. J. Proline Editing: A General and Practical Approach to the Synthesis of Functionally and Structurally Diverse Peptides. Analysis of Steric versus Stereoelectronic Effects of 4-Substituted Prolines on Conformation within Peptides. *J. Am. Chem. Soc.* **2013**, *135* (11), 4333–4363. DOI: 10.1021/ja3109664

(35) Lewis, J. E. M.; Tarzia, A.; White, A. J. P.; Jelfs, K. E. Conformational Control of Pd_2L_4 Assemblies with Unsymmetrical Ligands. *Chem. Sci.* **2020**, *11* (3), 677–683. DOI: 10.1039/C9SC05534G

(36) Brightwell, D. F.; Samanta, K.; Muldoon, J.; Fleming, P. C.; Ortin, Y.; Mardiana, L.; Waddell, P. G.; Hall, M. J.; Clark, E. R.; Fantuzzi, F.; Palma, A. *ChemRxiv* **2024**. This is a preprint and has not been peer-reviewed. DOI: 10.26434/chemrxiv-2024-wv36k

(37) Behrendt, R.; White, P.; Offer, J. Advances in Fmoc Solid-phase Peptide Synthesis. *J. Pept. Sci.* **2016**, *22* (1), 4–27. DOI: 10.1002/psc.2836

(38) Bhatt, M. R.; Zondlo, N. J. Electronic Control of Polyproline II Helix Stability via the Identity of Acyl Capping Groups: The Pivaloyl Group Particularly Promotes PPII. *Chem. Eur. J* **2024**, *30* (41), e202401454. DOI: 10.1002/chem.202401454

(39) Kuemin, M.; Engel, J.; Wennemers, H. Temperature-induced Transition between Polyproline I and II Helices: Quantitative Fitting of Hysteresis Effects. *J. Pept. Sci.* **2010**, *16* (10), 596–600. DOI: 10.1002/psc.1245

(40) Lewis, J. E. M.; Gavey, E. L.; Cameron, S. A.; Crowley, J. D. Stimuli-Responsive Pd_2L_4 Metallosupramolecular Cages: Towards Targeted Cisplatin Drug Delivery. *Chem. Sci.* **2012**, *3* (3), 778–784. DOI: 10.1039/C2SC00899H

(41) Ujma, J.; De Cecco, M.; Chepelin, O.; Levene, H.; Moffat, C.; Pike, S. J.; Lusby, P. J.; Barran, P. E. Shapes of Supramolecular Cages by Ion Mobility Mass Spectrometry. *Chem. Commun.* **2012**, *48* (37), 4423–4425. DOI: 10.1039/C2CC30778B

(42) Lewis, J. E. M. Multi-functional, Low Symmetry Pd_2L_4 Nanocage Libraries. *Chem. Eur. J.* **2021**, *27* (13), 4454–4460. DOI: 10.1002/chem.202005363

(43) Tarzia, A.; Lewis, J. E. M.; Jelfs, K. E. High-Throughput Computational Evaluation of Low Symmetry Pd_2L_4 Cages to Aid in System Design. *Angew. Chem. Int. Ed.* **2021**, *60* (38), 20879–20887. DOI: 10.1002/anie.202106721

(44) Ruzza, P.; Siligardi, G.; Donella-Deana, A.; Calderan, A.; Hussain, R.; Rubini, C.; Cesaro, L.; Osler, A.; Guiotto, A.; Pinna, L. A.; Borin, G. 4-Fluoroproline Derivative Peptides: Effect on PPII Conformation and SH3 Affinity. *J. Pept. Sci.* **2006**, *12* (7), 462–471. DOI: 10.1002/psc.750

(45) Horng, J.; Raines, R. T. Stereoelectronic Effects on Polyproline Conformation. *Protein Sci.* **2006**, *15* (1), 74–83. DOI: 10.1110/ps.051779806

(46) Costantini, N. V.; Ganguly, H. K.; Martin, M. I.; Wenzell, N. A.; Yap, G. P. A.; Zondlo, N. J. The Distinct Conformational Landscapes of 4*S*-Substituted Prolines that Promote an *Endo* Ring Pucker. *Chem. Eur. J.* **2019**, *25* (48), 11356–11364. DOI: 10.1002/chem.201902382

(47) Lopes, J. L. S.; Miles, A. J.; Whitmore, L.; Wallace, B. A. Distinct Circular Dichroism Spectroscopic Signatures of Polyproline II and Unordered Secondary Structures: Applications in Secondary Structure Analyses. *Protein Sci.* **2014**, *23* (12), 1765–1772. DOI: 10.1002/pro.2558

(48) Löffler, S.; Lübben, J.; Krause, L.; Stalke, D.; Dittrich, B.; Clever, G. H. Triggered Exchange of Anionic for Neutral Guests inside a Cationic Coordination Cage. *J. Am. Chem. Soc.* **2015**, *137* (3), 1060–1063. DOI: 10.1021/ja5130379

(49) Zhu, R.; Lübben, J.; Dittrich, B.; Clever, G. H. Stepwise Halide-Triggered Double and Triple Catenation of Self-Assembled Coordination Cages. *Angew. Chem. Int. Ed.* **2015**, *54* (9), 2796–2800. DOI: 10.1002/anie.201408068

(50) Freye, S.; Michel, R.; Stalke, D.; Pawliczek, M.; Frauendorf, H.; Clever, G. H. Template Control over Dimerization and Guest Selectivity of Interpenetrated Coordination Cages. *J. Am. Chem. Soc.* **2013**, *135* (23), 8476–8479. DOI: 10.1021/ja403184a

(51) Tateishi, T.; Yasutake, Y.; Kojima, T.; Takahashi, S.; Hiraoka, S. Self-Assembly Process of a Quadruply Interlocked Palladium Cage. *Commun. Chem.* **2019**, *2* (1), 25. DOI: 10.1038/s42004-019-0123-6